Biointerface Research in Applied Chemistry
Open-Access Journal (ISSN: 2069-5837)

Article
Volume 14, Issue 3, 2024, 65
https://doi.org/10.33263/BRIAC143.065

Effect of Dy^{3+} Concentration on Structure and Photoluminescence of $Li_4Zn(PO_4)_2$ Ph osphor

Akinapally Naveen [1,2], M Venkateswarlu [1,*], M V V K Srinivas Prasad [1], Nakka Chandana [3], Kaki Venkateswara Rao [4], Ghanta Chandana [4], Yajjala Rama krishna [4], Gurram Giridhar [5,*]

[1] Department of Engineering Physics, College of Engineering, Koneru Lakshmaiah Education Foundation, Vaddeswaram, Guntur, A.P., India
[2] Department of Physics & Electronics, Chaitanya (Deemed to be University), Hanamkonda 506001, Telangana, India
[3] Department of Physics, Dr.B.R. Ambedkar Open University, Hyderabad-500033 Telangana
[4] Department of Engineering Physics, Andhra University College of Engineering, Andhra University, Visakhapatnam
[5] Department of Nanotechnology, Acharya Nagarjuna University, A.P., India
* Correspondence: drggiridhar@rediffmail.com, mvrmphil@gmail.com;

Scopus Author ID 23972881700
Received: 28.07.2023; Accepted: 16.11.2023; Published: 17.02.2024

Abstract: A novel Dy^{3+}-activated $Li_4Zn(PO_4)_2$ phosphor was successfully prepared and characterized using various spectroscopic techniques. X-ray diffraction (XRD) patterns confirmed the single-phase $Li_4Zn(PO_4)_2$ structure, which agreed with the standard data. Energy-dispersive X-ray spectroscopy (EDS) also confirmed the presence of elements as per composition. Photoluminescence (PL) excitation spectra showed strong and narrow peaks in the ultraviolet (UV) region due to the 4f-4f transitions of the dopant ions. PL emission in the visible region with two intense emission lines showed concentration quenching of Dy^{3+} ions on emission intensity upon excitation. $Li_4Zn(PO4)_2$:0.05Dy^{3+} was optimized as a potential candidate for white light emission applications with multipole interaction. Decay profiles were also studied for all the concentrations of Dy^{3+}. Calculated color coordinates were well positioned in the white light region.

Keywords: phosphates; phosphor; white light generation; photoluminescence; decay profiles.

© 2024 by the authors. This article is an open-access article distributed under the terms and conditions of the Creative Commons Attribution (CC BY) license (https://creativecommons.org/licenses/by/4.0/).

1. Introduction

Solid-state lighting technology is the only solution for replacing conventional lighting with low-cost, high-efficiency, and eco-friendly alternatives. However, developing white LEDs with high-level features requires further research into obtaining tunable and efficient colors. These LEDs can be created by combining blue or near-ultraviolet excitation chips with a phosphor. Rare-earth-activated phosphor materials are important in various applications, such as bioimaging, temperature sensing, optical heating, and bio-thermal treatment, due to their intense and narrow bandwidth emissions. Dy^{3+} ions are a type of rare-earth ion with properties such as many energy states, emission bands in the blue, yellow, and weak red regions, importance in artificial photosynthesis, and high color purity. The choice of host material is also important for achieving efficient and single-phase white light emission from Dy^{3+} ions. Phosphates are one of the best host materials [1] for rare-earth ions as luminescent materials. They are eco-friendly, low-cost, have flexible PO_4 tetrahedral coordination, and are commercially used in display panels [2,3]. Additionally, when used as luminescent hosts,

phosphates with alkali and/or alkaline earth metals exhibit a wide bandgap in the ultraviolet region with reasonable phonon energy [4,5].

Researchers are developing new white light-emitting phosphors doped with Dy^{3+} in various hosts [6–12], including phosphates, for better performance when combined with near-ultraviolet (nUV) chips. In most studies, the emission intensity increases as the concentration of the activator increases. However, at higher concentrations, concentration quenching may occur due to the replacement of host atoms with activators. No reports show a reduction in emission intensity at low activator concentrations. Therefore, developing a new multi-component, low-cost, and eco-friendly host matrix is important to study the environment around dopant ions at lower concentrations. This study focuses on synthesizing a new $Li_4Zn(PO_4)_2$ phosphate phosphor and its luminescence characteristics.

In this work, a novel Dy^{3+}-doped $Li_4Zn(PO_4)_2$ phosphor was successfully prepared using combustion synthesis. The crystal structure, phase purity, surface morphology, and emission behavior with decay profiles of the phosphor were studied. The dopant concentration dependency was also investigated. The results showed that the dopant concentration had a significant effect on the emission behavior of the phosphor. Further, this study suggests that Dy^{3+}-doped $Li_4Zn(PO_4)_2$ phosphor is a promising candidate for white light emission applications. Further studies are needed to optimize the phosphor for practical applications.

2. Materials and Methods

$Li_4Zn(PO_4)_2$:xDy^{3+} (where x = 0.01, 0.03, 0.05, 0.08, and 0.1mol%) phosphors were prepared using the combustion method. Stoichiometric amounts of all materials were taken along with urea as fuel and H_3BO_3 as flux. X-ray diffraction measurements were performed using a SHIMADZU LabX DRD-6100 diffractometer. Photoluminescence studies were carried out using a Thermo Lumina spectrophotometer. Lifetimes were measured using an Edinburgh Instruments FLSP 920 system. FTIR spectra were recorded using a BRUKER Compact spectrophotometer. All characterizations were performed at room temperature.

3. Results and Discussion

Figure 1 shows the X-ray diffraction (XRD) patterns of a new $Li_4Zn(PO_4)_2$ (pure) and doped $Li_4Zn(PO_4)_2$:xDy^{3+} (where x = 0.01, 0.03, 0.05, 0.08, and 0.1) phosphors. The peaks obtained are in good agreement with the standard monoclinic structure of $Li_4Zn(PO_4)_2$ with P21(4) space group (JCPDS Card No01-73-0622). The absence of any other phases suggests that all the composed elements are properly positioned in the host due to the high internal temperatures produced in the combustion method. This is important for phosphors, as it ensures that the dopant ions are evenly distributed throughout the host lattice, which is necessary for efficient emission. The XRD patterns also show that the peak intensities increase with increasing dopant concentration. This is expected, as the more dopant ions there are, the more likely they interact with the host lattice and emit light. The emission intensity of the doped phosphors is also higher than that of the pure phosphor, which is another desirable property for white light applications.

The highest intensity peak was observed at $2\theta = 22.131^{o}$, corresponding to the (-1 1 2) plane. The crystallite sizes were calculated by using standard Debye-Scherrer's formula (Eq.(1))

$$D = \frac{0.9\,\lambda}{\beta Cos\theta} \qquad (1)$$

where D-crystallite size, β-full width half maximum, λ – x-ray wavelength. The calculated crystallite sizes for the phosphors are shown in Table 1.

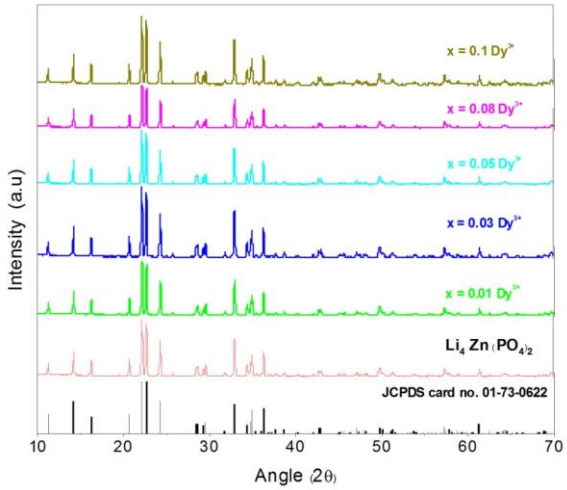

Figure 1. X-ray diffraction patterns of $Li_4Zn(PO_4)_2$:xDy^{3+} with standard structure.

Table 1. Crystallite sizes from the x-ray diffraction patterns for the present phosphors.

Phosphor	Crystallite size (nm)
$Li_4Zn(PO_4)_2$ -Pure	82
$Li_4Zn(PO_4)_2$:0.01Dy^{3+}	83
$^{+}$ $Li_4Zn(PO_4)_2$:0.03Dy^{3}	82
$Li_4Zn(PO_4)_2$:0.05Dy^{3+}	89
$Li_4Zn(PO_4)_2$:0.08Dy^{3+}	95
$Li_4Zn(PO_4)_2$:0.1Dy^{3+}	93

The crystallite sizes of the pure $Li_4Zn(PO_4)_2$ and doped phosphors are not significantly different. This suggests that the Dy^{3+} ions are incorporated into the host lattice homogeneously. However, there are small variations in the electronic density of the lattice due to the presence of the dopant ions. These variations lead to a small change in the peak intensities of the XRD patterns. Moreover, no evidence of broadening or large peak shifts suggests that the doping does not significantly distort the crystal structure. The refinement of the X-ray diffraction pattern ($Li_4Zn(PO_4)_2$:0.1 Dy^{3+}) is shown in Figure 2.

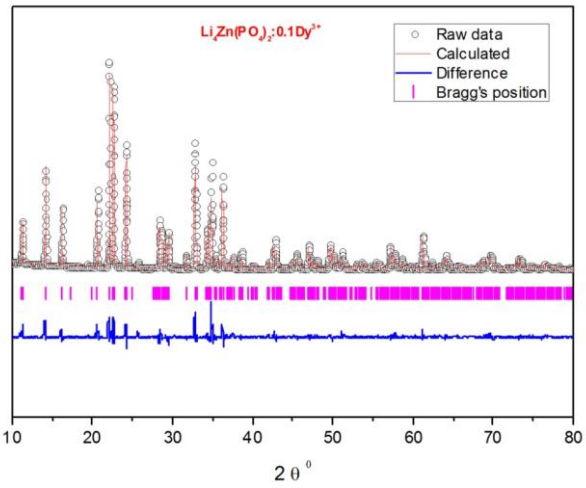

Figure 2. Reitveld refinement of the $Li_4Zn(PO_4)_2$:0.1Dy^{3+} phosphor.

The crystal parameters of $Li_4Zn(PO_4)_2$ are a=8.103Å, b=10.276Å, c=8.121Å, and β=104.871°. As shown in Figure 2, the experimental diffraction peaks agree well with the

calculated data. The refined crystallographic parameters, reliability factors, and structural parameters are a=8.118Å, b=10.288Å, c=8.134Å, and β=104.832°. The reliability factors are R_p=12.24%, R_{wp}=11.43%, and χ^2=6.532. These values indicate that the prepared phosphor is pure in phase.

The doped Dy^{3+} ions are positioned at the faces of the crystal structure. The crystal structure of $Li_4Zn(PO_4)_2$ was developed using the VESTA software and is shown in Figure 3.

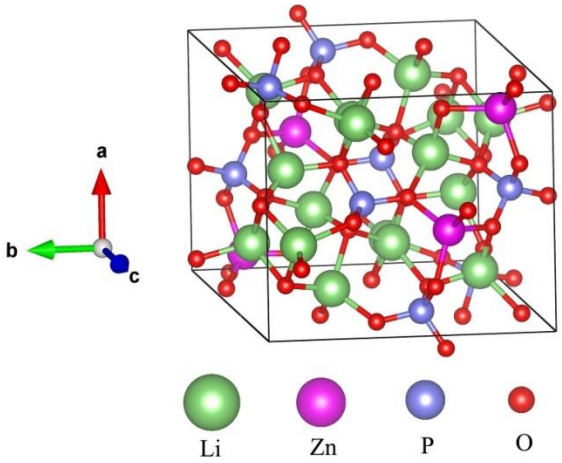

Figure 3. Crystal structure of $Li_4Zn(PO_4)_2$ host lattice.

Scanning electron microscopy (SEM) images with energy-dispersive X-ray spectroscopy (EDS) are shown in Figure 4. The images clearly show the agglomeration and irregular shapes of the phosphors, which are attributed to the high temperatures of the combustion synthesis method. EDS confirms the presence of all the elements in $Li_4Zn(PO_4)_2$. However, due to the instrument's limitations, Li could not be detected, as it is a light element with an atomic number of 3.

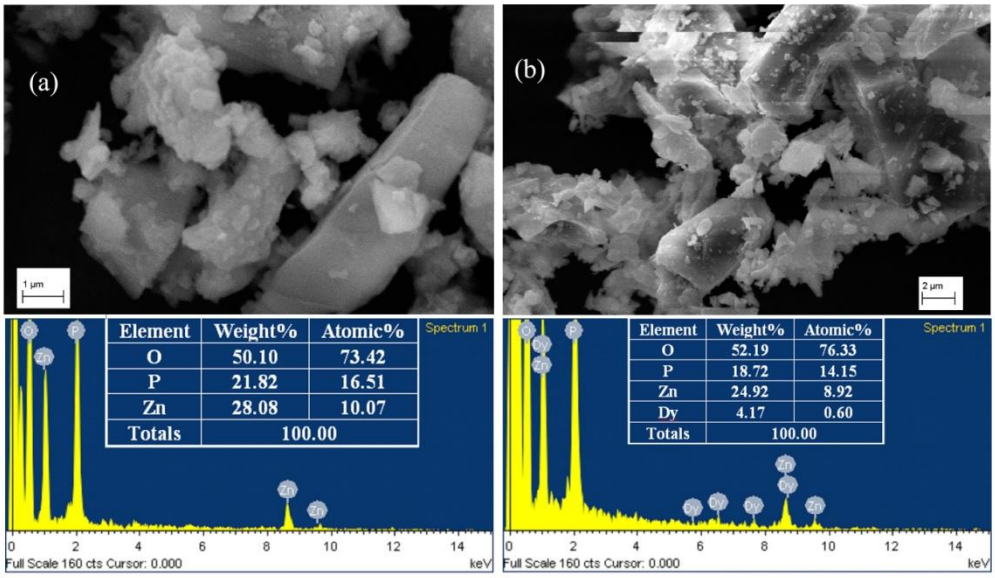

Figure 4. SEM images and EDS details of pure $Li_4Zn(PO_4)_2$ and $Li_4Zn(PO_4)_2$:0.1Dy^{3+}.

EDS shows that Dy is well associated with Zn, supporting the intensity variations observed in the X-ray diffraction patterns. The association of Dy with Zn is important for the emission properties of the phosphors. Dy^{3+} is a rare-earth element with a strong emission in the blue region of the visible spectrum. When Dy^{3+} is doped into the $Li_4Zn(PO_4)_2$ lattice, it can trap electrons excited by light. When these electrons relax, they emit blue light. The emission

of blue light makes the phosphors useful for applications such as white light emission. The agglomeration of the phosphors is a disadvantage, as it can lead to poor light output and uneven emission. However, the agglomeration can be reduced by optimizing the synthesis conditions.

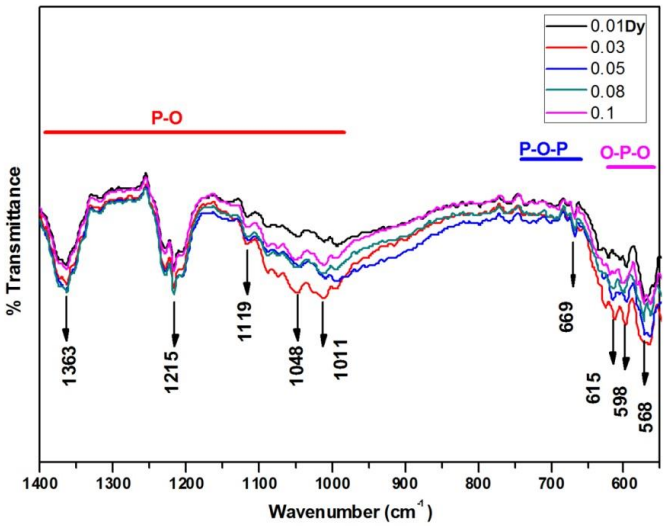

Figure 5. FTIR spectra of $Li_4Zn(PO_4)_2$:xDy^{3+} phosphors.

The FTIR spectra of the phosphate glasses under study are shown in Fig 5. The spectra exhibit almost similar bond natures, with dominant nine bands at ~568cm^{-1}, ~598cm^{-1},~615cm^{-1}, ~669cm^{-1}, ~1011cm^{-1}, ~1048cm^{-1}, ~1119cm^{-1},~1215cm^{-1} and ~1363cm^{-1}. These bands indicate that the phosphate glasses are composed of cross-linked PO_4 tetrahedra with terminal double-bonded oxygen and three bridging oxygen. The relative intensities of the bands can be used to assess the structural changes in the glasses due to composition variations [13]. The bands assigned for the observed vibrations are ~ $(PO_4)^{3-}$ for 568 and 598cm^{-1}[14], $(P\text{-}O\text{-}P)_{sym}$ for 615 and 669cm^{-1}, $(PO_4)^{3-}$ for 1011cm^{-1} [15], P-O stretching for 1048cm^{-1} [14,16], $(PO_3)_{as}$ stretching vibration for 1119cm^{-1} [17], $(PO_2)_{as}$ vibration for 1220 cm^{-1} and P-O stretching of pyrophosphates for 1360cm^{-1} [13,14,18] respectively.

Although the influence and contribution of dysprosium and alkali earth content are shown by FTIR spectra, there is no clear proof of their presence. It is clear that neither the number nor the position of the bands changed noticeably due to the addition of alkali earth content. However, due to the incorporation of Dy^{3+} ions into the matrix, which creates non-bridging oxygen, the only minute changes that can be seen are a relative rise in intensities and a tiny shift in the bands.

Fig. 6 shows the excitation and emission behavior with decay profiles as a concentration of Dy^{3+} ions. Here in Fig 6a, excitation spectra monitored at 573nm show an intense peak at 348nm as the highest population level, and the others are with lower intensities and are assigned to various transitions from the ground state $^6H_{15/2}$. The transition $^6H_{15/2} \rightarrow {}^6P_{7/2}$ corresponding to 348 nm is preferred as an excitation wavelength to record emission spectra for the current single phase $Li_4Zn(PO_4)_2$ phosphor. Further, this wavelength is more suitable for the fabrication of UV-pumped phosphor LEDs [19–29]. Fig 6b, emission spectra of $Li_4Zn(PO_4)_2$ phosphors consist of two intense bands for all the concentrations of Dy^{3+} ions [12,30]. The two emission bands corresponding to the transitions $^4F_{9/2} \rightarrow {}^6H_{15/2}$ and $^4F_{9/2} \rightarrow {}^6H_{13/2}$ are centered at 483nm and 573nm, respectively. The Energy level diagram with the excitation and emission lines for Dy^{3+} ions is shown in Fig 7.

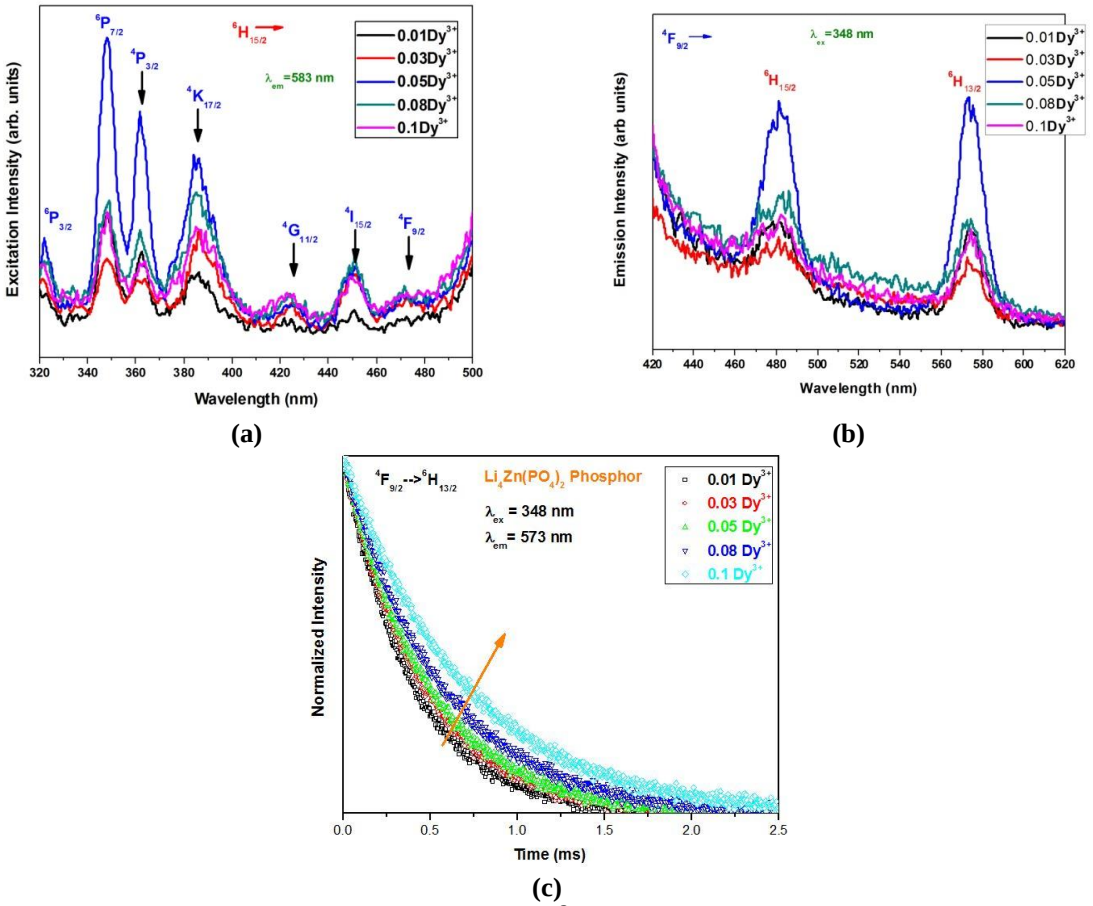

Figure 6. (**a**) Excitation behavior of $Li_4Zn(PO_4)_2$:Dy^{3+} phosphor; (**b**) Emission behavior of $Li_4Zn(PO_4)_2$:Dy^{3+} phosphor; (**c**) Decay profiles of Dy^{3+} doped $Li_4Zn(PO_4)_2$ phosphor.

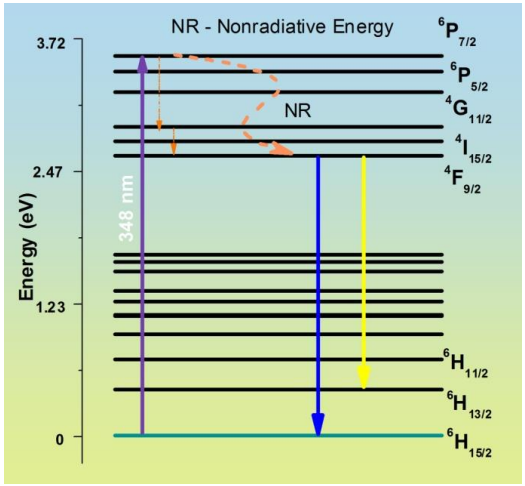

Figure 7. Energy level diagram of Dy^{3+} ion in $Li_4Zn(PO_4)_2$ host.

The band in the blue region corresponds to $^4F_9 \rightarrow {}^6H_{15/2}$ transition is a magnetic dipole transition ($\Delta J = 0, \pm 1$, but $0 \leftrightarrow 0$ forbidden) and is less sensitive to the surrounding environment of Dy^{3+} ions. The other intense band in the yellow region corresponds to $^4F_9 \rightarrow {}^6H_{13/2}$ transitions ($\Delta J = \pm 2$ and $\Delta L \pm 2$) is an electric dipole transition and is hypersensitive. Its intensity strongly depends on the environment around Dy^{3+} ions [27,31,32]. The emission spectra also suggest the low symmetry site occupancy of Dy^{3+} ions, as the peak intensity in the yellow region is higher than in the blue region. This yellow-to-blue (Y/B) intensity ratio suggests a higher degree of covalence between Dy^{3+} and its oxygen ligands. Moreover, except for intensity variation, no major shift in the position of the emission bands with the concentration variation

of Dy^{3+} occurred. The intensity increases up to x=0.05mol% Dy^{3+}; after that, it decreases in this $Li_4Zn(PO_4)_2$ host. This could be due to the interaction between donor and acceptor ions and resonance energy transfer between activator ions below the self-quenching limits and can be referred to as luminescence quenching. The reduction in intensity occurs due to the multipolar interactions referred to as dipole-dipole interactions or dipole-quadrupole interactions [33]. Further, the slight marginal shifts are due to the divergence of ligand filed with the host matrix [29].

In the present study, for 0.05mol% of Dy^{3+} ions, maximum photoluminescence intensity occurred. Hence, 0.05 mol% is the best doping concentration in the $Li_4Zn(PO_4)_2$ host, and the corresponding energy level diagram of Dy^{3+} ions is shown in Fig. 7.

Fig 6c shows the decay profiles of $Li_4Zn(PO_4)_2$:xDy^{3+} phosphors where x=0.01, 0.03, 0.05, 0.08 and 0.1. All the profiles were monitored at 348nm and 573nm as excitation and emission wavelengths, respectively. All the profiles are fitted, and the lifetimes are estimated by a first-order exponential decay equation given in Eq (1a).

$$I(t) = I(0)\exp\left(\frac{-t}{\tau}\right) \qquad (1a)$$

where *I* (t) and *I* (0) are the emission intensities at time *t* and 0, respectively, *A* is a constant, *t* is time, and τ is the decay time for an exponential component.

The estimated lifetimes are 0.482, 0.538, 0.556, 0.0.592 and 0.641ms for x= 0.01, 0.03, 0.05, 0.08 and 0.1mol% of Dy^{3+} ion. Lifetimes are slightly increased with the concentration of Dy^{3+} ions and are attributed to the reduction in non-radiative transitions and separation between Dy^{3+} ions [34,26]. The quenching in emission intensity is caused by the cross-relaxation between neighboring activator ions [35]. Sometimes, these intensities were dependent on crystallite sizes as the particle unit area facing towards the incident light results in higher intensities at smaller crystallite sizes [36,37]. So, the inhomogeneous distribution of dopants in the host matrix creates variations in the local environment, which can lead to a consequent increase in lifetime with increasing dopant concentration. Therefore, both cross-relaxation and crystallite sizes are influencing the present $Li_4Zn(PO_4)_2$:xDy^{3+} phosphor system.

The performance of the prepared phosphors is estimated by the CIE 1931 (Commission Internationale de I'Eclairage) color coordinates (x, y) by using Eq. (2) from the tri-stimulus values.

$$x = \frac{X}{X+Y+Z} \qquad (2a)$$

$$y = \frac{Y}{X+Y+Z} \qquad (2b)$$

where *X,Y,* and *Z* are the color-matching functions for primary red, green and blue colors to match the color of $P(\lambda)$. The color-matching functions can be evaluated using the following equations [38]

$$X = \int_{\lambda} \bar{x}(\lambda)P(\lambda)d\lambda \qquad (3a)$$

$$Y = \int_{\lambda} \bar{y}(\lambda)P(\lambda)d\lambda \qquad (3b)$$

$$Z = \int_{\lambda} \bar{z}(\lambda)P(\lambda)d\lambda \qquad (3c)$$

Further, color purity is also an important parameter estimated using Eq.(4) with (x,y) color coordinates and standard values. The expression to evaluate the color purity is:

$$\text{Color purity} = \frac{\sqrt{(x-x_{ee})^2+(y-y_{ee})^2}}{\sqrt{(x_d-x_{ee})^2+(y_d-y_{ee})^2}} \quad (4)$$

where $(x, y), (x_{ee}, y_{ee})$ are the chromaticity coordinates of the emission light and equal energy point and (x_d, y_d) are the dominant wavelength points.

All the parameters, such as color purity, CCT values, emission output, and visible power, are calculated by Color Calculator v.7.77 and presented in Table 2. Fig 8 shows the CIE diagram with all the obtained coordinates, and the inset shows the emission spectrum of 0.05 mol% Dy^{3+}.

Table 2. CIE color coordinates with purity.

Sample	x	y	CCT(K)	Lumens 10^{-20}	Visible power(mW) 10^{-19}	Color Purity(%)
0.01	0.2606	0.3292	9910	9.4	3.1	24.9
0.03	0.2599	0.3551	9098	9.8	3.0	23.5
0.05	0.2789	0.3455	8179	14	4.4	17.6
0.08	0.2601	0.3554	9078	13	4.2	23.4
0.1	0.2589	0.3410	9596	11	3.6	24.7

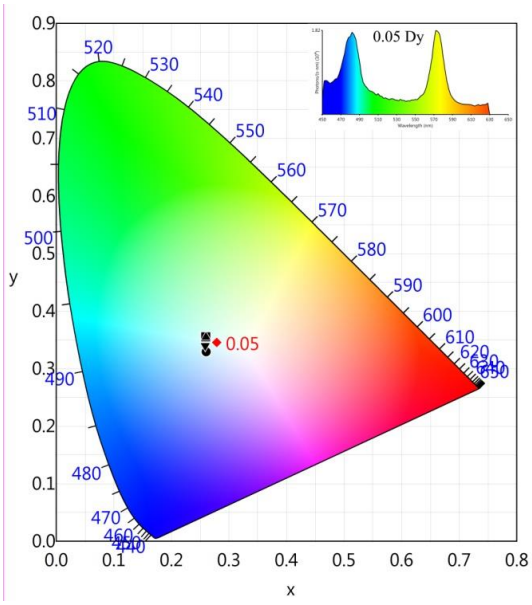

Figure 8. CIE diagram - $Li_4Zn(PO_4)_2$:xDy^{3+} phosphors.

All the coordinates are well placed in the white light region, and the 0.05 Dy^{3+} sample exhibits more prominent white light than others. The CCT values and color purity depend on the dopant concentration and excitation wavelength [39,40]. The obtained values for the $Li_4Zn(PO_4)_2$:xDy^{3+} phosphors are in correlation to pure white light (0.33, 0.33) [41]. Particularly, 0.05mol% of Dy^{3+} sample emits more pure white light than others and can be optimized.

Overall, the studies reveal that the present $Li_4Zn(PO_4)_2$ host is suitable for accepting rare earth ions with crystal field effects. So, this kind of single-phased hosts are very useful in the fabrication of display, and lighting devices.

4. Conclusions

A series of Dy^{3+} doped $Li_4Zn(PO_4)_2$ phosphors are synthesized. X-ray diffraction spectra confirm the phase purity and crystal structure of phosphors. Dy^{3+} single doped $Li_4Zn(PO_4)_2$ phosphor emits light in blue and yellow regions. Variation in emission intensities due to dy^{3+} concentration is attributed to the local crystal structure/crystal field around Dy^{3+} ions and separation between activator ions. The CIE diagram shows excellent white light emission with high color purity. Therefore, Dy^{3+} doped $Li_4Zn(PO_4)_2$ phosphors are potentially useful in fabricating display and white light emitting devices.

Funding

This research received no external funding.

Acknowledgments

The authors thank the Department of Physics, KLCE, Vaddeswaram, and Guntur for providing an X-ray diffraction facility.

Conflicts of Interest

The authors have declared no conflict of interest.

References

1. Gao, M.; Li, K.; Yan, Y.; Xin, S.; Dai, H.; Zhu, G.; Wang, C. Novel thermally robust warm white light emitting phosphor$Ca_{18}Li_3Y(PO_4)_{14}:Dy^{3+}$: Synthesis, crystal structure and luminescence property investigation. *J. Mol. Struct.* **2021**, *1228*, 129471, https://doi.org/10.1016/j.molstruc.2020.129471.
2. Yu, L.; Song, H.; Liu, Z.; Yang, L.; Zheng, S.L.Z. Electronic Transition and Energy Transfer Processes in $LaPO_4:Ce^{3+}/Tb^{3+}$ Nanowires. *J. Phys. Chem. B* **2005**, *109*, 11450–11455, http://doi.org/10.1021/jp045238e.
3. Wu, C.-C.; Chen, K.-B.; Lee, C.-S.; Chen, T.-M.; Cheng, B.-M. Synthesis and VUV Photoluminescence Characterization of $(Y,Gd)(V,P)O_4:Eu^{3+}$ as a Potential Red-Emitting PDP Phosphor. *Chem. Mater*. **2007**, *19*, 3278–3285, http://doi.org/10.1021/cm061042a.
4. Raju, G.S.R.; Pavitra, E.; Yu, J.S. Luminescence properties of Dy^{3+} ions activated novel warm white-light emitting $CaGd_2ZnO_5$ nanophosphors. *Ceram. Int.* **2015**, *41*, 11228–11233, https://doi.org/10.1016/j.ceramint.2015.05.073.
5. Wu, Z.; Liu, J.; Guo, Q.; Gong, M. A Novel Blue-green-Emitting Phosphor $LiBaPO_4$: Eu^{2+} for White Light-emitting Diodes. *Chem. Lett.* **2008**, *37*, 190–191, https://doi.org/10.1246/cl.2008.190.
6. Li, Y.; Dai, S.; Zhang, W.; Zhang, P.; Qiu, K. Enhancement of the luminescence properties of $Sr_3(PO_4)_2:Dy^{3+},Li^+$ white-light-emitting phosphors by charge compensator Li^+ co-doping. *Luminescence* **2017**, *32*, 1593–1596, https://doi.org/10.1002/bio.3387.
7. Yu, M.; Zhang, W.; Yan, G.; Dai, S.; Qiu, Z.; Zhang, L. Warm white emission property of $Ca_2Sr(PO_4)_2:Dy^{3+}$ phosphors with red compensation byEu^{3+} co-doping. *Ceram. Int.* **2018**, *44*, 2563–2567, http://doi.org/10.1016/j.ceramint.2017.11.012.
8. Dai, S.; Zhang, W.; Zhou, D.; Yan, G.; Liu, S. Effect of A^+ (A= Li, Na and K) co-doping on the luminescence enhancement of $CaSr_2(PO_4)_2$: Dy^{3+} phosphors for white light-emitting diodes. *Ceram. Int.* **2017**, *43*, 15493–15499, https://doi.org/10.1016/j.ceramint.2017.08.097.
9. Hu, S.; Qin, X.; Zhou, G.; Liu, X.; Lu, C.; Xu, Z.; Wang, S. Effect of doping concentration on particle growth and luminescence properties of monodispersed Dy^{3+}: Y_2O_3. *J. Alloys Compd.* **2016**, *664*, 304–310, https://doi.org/10.1016/j.jallcom.2015.12.207.
10. Cao, R.; Zheng, Y.; Chen, T.; Lan, B.; Li, L.; Zhong, Q.; Nie, S.; Wang, J. Synthesis and tunable emission from yellow-green to red-orange of $Ca_3MgSi_2O_8$: Eu^{3+}, Dy^{3+} phosphor. *J. Mol. Struct.* **2022**, *1262*, 133008, https://doi.org/10.1016/j.molstruc.2022.133008.

11. Saraswathi, A.V.; Prabhu, N.S.; Naregundi, K.; Sayyed, M.I.; Murari, M.S.; Almuqrin, A.H.; Kamath, S.D. Thermoluminescence investigations of $Ca_2Al_2SiO_7$: Dy^{3+} phosphor for gamma dosimetry applications. *Mater. Chem. Phys.* **2022**, *281*, 125872, https://doi.org/10.1016/j.matchemphys.2022.125872.
12. Ravi, M.; Chakrapani, G.P.; Balachandrika, M.; Vasudevarao, P.; Nageswararao, C.; Babu, L.K.K.; Prasad, P.M.; Giridhar, G. Photoluminescence studies on $LiNa_5(PO_4)_2$: Dy^{3+}, Sm^{3+} phosphor. *Z. Für Naturforschung A* **2022**, *77*, 279–290, https://doi.org/10.1515/zna-2021-0153.
13. Raynaud, S.; Champion, E.; Bernache-Assollant, D.; Thomas, P. Calcium phosphate apatites with variable Ca/P atomic ratio I. Synthesis, characterisation and thermal stability of powders. *Biomaterials* **2002**, *23*, 1065–1072, https://doi.org/10.1016/S0142-9612(01)00218-6.
14. Destainville, A.; Champion, E.; Bernache-Assollant, D.; Laborde, E. Synthesis, characterization and thermal behavior of apatitic tricalcium phosphate. *Mater. Chem. Phys.* **2003**, *80*, 269–277, https://doi.org/10.1016/S0254-0584(02)00466-2.
15. Patel, N.P.; Srinivas, M.; Verma, V.; Modi, D. The effect of Tb^{3+} on α-$Sr_2P_2O_7$ phosphor for green LED phosphor application. *AIP Conf. Proc.* **2015**, *1665*, 110017, https://doi.org/10.1063/1.4918073.
16. Debnath, S.; Saxena, S.K.; Nagabhatla, V. Facile synthesis of crystalline nanoporous $Mg_3(PO_4)_2$ and its application to aerobic oxidation of alcohols. *Catal. Commun.* **2016**, *84*, 129–133, https://doi.org/10.1016/j.catcom.2016.06.018.
17. Lai, Y.M.; Liang, X.F.; Yang, S.Y.; Wang, J.X.; Cao, L.H.; Dai, B. Raman and FTIR spectra of iron phosphate glasses containing cerium. *J. Mol. Struct.* **2011**, *992*, 84–88, https://doi.org/10.1016/j.molstruc.2011.02.049.
18. Zhang, Z.-w.; Wu, Y.-n.; Shen, X.-h.; Ren, Y.-j.; Zhang, W.-g.; Wang, D.-j. Enhanced novel orange red emission in $Ca_3(PO_4)_2$:Sm^{3+} by harge compensation. *Opt. Laser Technol.* **2014**, *62*, 63–68, https://doi.org/10.1016/j.optlastec.2014.02.014.
19. Pradhan, M.K.; Rao, T.L.; Dash, S. Dy^{3+} Activated Nearly White Emitting $NaCdPO_4$ as Potential Phosphors for Solid State Light Applications. *J. Electron. Mater.* **2020**, *49*, 2463–2470, http://doi.org/10.1007/s11664-020-07954-w.
20. Yu, M.; Xu, X.; Zhang, W.; Chen, X.; Zhang, P.; Huang, Y. The effect of Sm^{3+} co-doping on the luminescence properties of $Ca_{2\cdot85}Li_{0\cdot15}$ $(PO_4)_{1\cdot85}(SO_4)_{0.15}$: Dy^{3+} white-emitting phosphors. *J. Alloys Compd.* **2020**, *817*, 152761, https://doi.org/10.1016/j.jallcom.2019.152761.
21. Yu, M.; Zhang, W.; Yan, G.; Dai, S.; Qiu, Z.; Zhang, L. Warm white emission property of $Ca_2Sr(PO_4)_2$: Dy^{3+} phosphors with red compensation by Eu^{3+} co-doping. *Ceram. Int.* **2018**, *44*, 2563–2567, https://doi.org/10.1016/j.ceramint.2017.11.012.
22. Liu, S.; Liu, S.; Wang, J.; Sun, P.; Zhong, Y.; Jeong, J.H.; Deng, B.; Yu, R. Preparation and investigation of Dy^{3+}-doped $Ca_9LiGd_{2/3}(PO_4)_7$ single-phase full-color phosphor. *Mater. Res. Bull.* **2018**, *108*, 275–280, http://doi.org/10.1016/j.materresbull.2018.08.026.
23. Zhang, Y.; Gong, W.; Yu, J.; Pang, H.; Song, Q.; Ning, G. A new single-phase white-light-emitting $CaWO_4$:Dy^{3+} phosphor: synthesis, luminescence and energy transfer. *RSC Adv.* **2015**, *5*, 62527–62533, https://doi.org/10.1039/C5RA12502B.
24. Nagpure, I.M.; Pawade, V.B.; Dhoble, S.J. Combustion synthesis of $Na_2Sr(PO_4)F$: Dy^{3+} white light emitting phosphor. *Luminescence* **2010**, *25*, 9–13, https://doi.org/10.1002/bio.1132.
25. Huerta, E.F.; Meza-Rocha, A.N.; Lozada-Morales, R.; Speghini, A.; Bordignon, S.; Caldiño, U. White, yellow and reddish-orange light generation in lithium-aluminum-zinc phosphate glasses co-doped with Dy^{3+}/Tb^{3+} and tri-doped with Dy^{3+}/Tb^{3+}/Eu^{3+}. *J. Lumin.* **2020**, *219*, 116882, http://doi.org/10.1016/j.jlumin.2019.116882.
26. Liu, S.; Yuan, H.; Feng, Y.; Sun, X. The synthesis and photoluminescence characteristics Bi^{3+}/Dy^{3+} doped Ca_2LaTaO_6 phosphors upon the NUV light excitation. *J. Lumin.* **2021**, *238*, 118327, http://doi.org/10.1016/j.jlumin.2021.118327.
27. Krishnapriya, T.; Mohan P.R.; Jose, A.; Jose, J.R.; Joseph, C.; Biju, P.R. Synthesis and luminescence characteristics of $Na_6Ca_{(1-X)}P_2O_9$:XDy^{3+} phosphor for outdoor lighting applications. *Mater. Chem. Phys.* **2022**, *280*, 125827, https://doi.org/10.1016/j.matchemphys.2022.125827.
28. Kohale, R.L.; Dhoble, S.J. Spectroscopic investigations of Dy^{3+} activated $MCaP_2O_7$ (M= Sr/Ba) pyrophosphate phosphors. *J. Alloys Compd.* **2018**, *753*, 111–118, https://doi.org/10.1016/j.jallcom.2018.04.192.

29. Duragkar, A.; Kohale, R.L.; Dhoble, N.S.; Dhoble, S.J. Tunable luminescence of Eu^{3+}, Sm^{3+} and Dy^{3+} doped $Na_2CaMg(PO_4)_2$ phosphor for optical applications. *J. Mol. Struct.* **2020**, *1199*, 126969, http://doi.org/10.1016/j.molstruc.2019.126969.
30. Xie, M.; He, C.; Fang, M.; Huang, Z.; Liu, Y.; Wu, X.; Min, X. Improvement of luminescence performance of single-phase white-emitting $Na_3Gd(PO_4)_2$:Dy^{3+} phosphor by co-doping with Eu^{3+}. *Polyhedron* **2022**, *222*, 115860, https://doi.org/10.1016/j.poly.2022.115860.
31. Kumar, G.K.; Bhargav, B.P.; Aravinth, K.; Ramasamy, P.; Sen, S.; Arumugam, R. Tunable photoluminescence properties of Dy^{3+} doped LLZO phosphors for WLED and dosimetry applications *Ceram. Int.* **2022**, *48*, 1402–1407, https://doi.org/10.1016/j.ceramint.2021.09.226.
32. Khajuria, P.; Manhas, M.; Bedyal, A.K.; Vij, A.; Swart, H.C.; Kumar, V. Structural and spectral investigation of a near-UV-converted $LiSrP_3O_9$:Dy^{3+} spectral investigation of a near-UV-converted *J. Mater. Sci. Mater. Electron.* **2022**, *33*, 6031–6042, http://doi.org/10.1007/s10854-022-07782-0.
33. Manik, U.; Gedam, S.C.; Dhoble, S.J. The characterization and mechanism of energy transfer in $Na_2Mg(SO_4)_2$: Ce phosphor co-doped by Dy, Mn and Tb. *J. Lumin.* **2013**, *136*, 191–195, https://doi.org/10.1016/j.jlumin.2012.10.029.
34. Qu, M.; Zhang, X.; Mi, X.; Liu, Q.; Bai, Z. Novel color tunable garnet phosphor of Tb^{3+} and Eu^{3+} co-doped $Ca_2YZr_2Al_3O_{12}$ with high thermal stability via energy transfer. *J. Alloys Compd.* **2020**, *828*, 154398, https://doi.org/10.1016/j.jallcom.2020.154398.
35. Matthews, L.R.; Wang, X.-j.; Knobbe, E.T. Concentration effects on the luminiscence behavior of europium (III) chloride- and organoeuropium-doped silicate gels. *J. Non-Cryst. Solids* **1994**, *178*, 44–51, https://doi.org/10.1016/0022-3093(94)90263-1.
36. Sharma, P.K.; Nass, R.; Schmidt, H. Effect of solvent, host precursor, dopant concentration and crystallite size on the fluorescence properties of Eu(III) doped yttria. *Opt. Mater.* **1998**, *10*, 161–169, https://doi.org/10.1016/S0925-3467(97)00140-7.
37. Iwasaki, S.; Ida, T.; Kimura, K. Blue-Green Photoluminescence from Ultrafine Colloidal Si Particles in 2-Propanol. *Jpn. J. Appl. Phys.* **1996**, *35*, L551, http://doi.org/10.1143/JJAP.35.L551.
38. Schubert, E.F.; Kim, J.K. Solid-State Light Sources Getting Smart. *Science* **2005**, *308*, 1274–1278, https://doi.org/10.1126/science.1108712.
39. Hakeem, D.A.; Pi, J.W.; Jung, G.W.; Kim, S.W.; Park, K. Structural and photoluminescence properties of $La_{1-X}NaCaGa_3PZrO_{12}$ Doped with Ce^{3+}, Eu^{3+}, and Tb^{3+}. *Dyes Pigments* **2019**, *160*, 234–242 https://doi.org/10.1016/j.dyepig.2018.06.047.
40. Hakeem, D.A.; Pi, J.W.; Kim, S.W.; Park, K. New $Y_2LuCaAl_2SiO_{12}$:Ln (Ln = Ce^{3+}, Eu^{3+} and Tb^{3+}) phosphors for white LED applications. *Inorg. Chem. Front.* **2018**, *5*, 1336-1345, https://doi.org/10.1039/C8QI00111A.
41. Ci, Z.; Sun, Q.; Qin, S.; Sun, M.; Jiang, X.; Zhang, X.; Wang, Y. Warm white light generation from a single phase Dy^{3+} doped $Mg_2Al_4Si_5O_{18}$ phosphor for white UV-LEDs. *Phy. Chem. Chem. Phy.* **2014**, *16*, 11597–11602, http://doi.org/10.1039/c4cp00357h.